



Cyclic and Monotonic Behavior of Non-plastic Silts with the Presence of Initial Static Shear Stress Using Strain Energy Approach: A Case Study for a Tailings Dam

M. Abdollahi, J. Bolouri Bazaz*, A. Akhtarpour

Civil Engineering Department, Ferdowsi University of Mashhad, Mashhad, Iran

PAPER INFO

Paper history:

Received 08 October 2023

Received in revised form 21 November 2023

Accepted 26 November 2023

Keywords:

Triaxial

Static Shear Stress Ratio

Liquefaction

Strain Energy

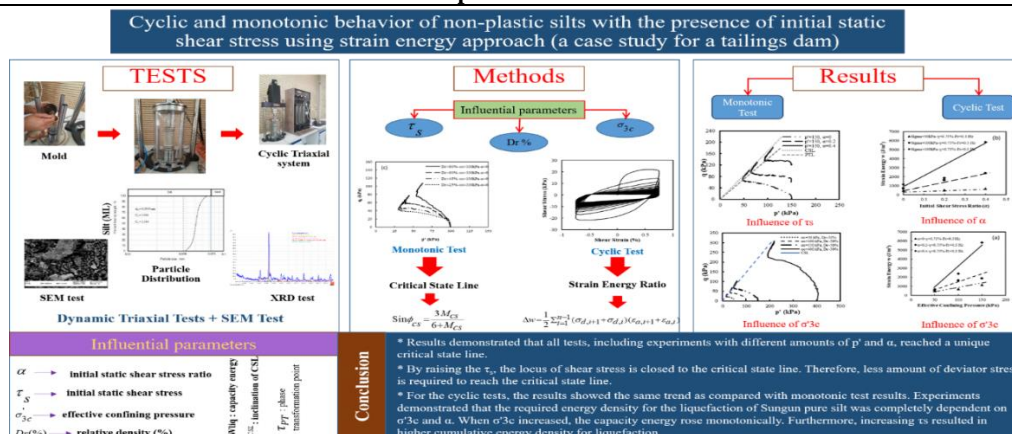
Non-plastic Silt

ABSTRACT

Mining Exploration, excavation, and construction are considered as mining activities which are recently growing dramatically. Therefore, utilizing the mining wastes with the least environmental damage is a significant concern. Tailings dams are one of the conventional solutions that store the extracted hazardous substances safely for water resources management and environmental protection. This research deals with the effects of monotonic and seismic loadings on silt-sized copper wastes existed in a tailings dam at Northwest Iran as a case study. Various values of initial static shear stress are performed using an automated cyclic triaxial system. Monotonic undrained compressive tests were performed with a relatively constant density and considering three values of 50, 100, and 150 kPa for mean effective stress. Depending on the first density of samples, applying a mean effective confining pressure of 100 kPa, increased the initial densities by 25 to 30% as compared to the initial condition. Moreover, the effect of initial shear stress ratio with three values of 0, 0.2, and 0.4 was evaluated. No peak point was observed for samples under $\alpha = 0$, whereas, samples with $\alpha = 0.4$ encountered a peak point before reaching to the phase transformation point. The results of cyclic experiments were used to evaluate capacity energy and residual pore pressure based on the strain energy approach. Cyclic tests on the samples were performed considering the shear amplitude of 0.75% and frequency of 0.3 Hz. It is shown that the most energy dissipation occurs at the first cycle possessing the highest stiffness. For $\alpha = 0$, energy density increased from 474 J/m³ to 1147.4 J/m³; however, a more intense increase was measured from 682 J/m³ to 5839 J/m³ when $\alpha = 0.4$. It is also found that applying initial shear stress has a pretty considerable influence on monotonic strength and the liquefaction resistance of silts. The increase of α from 0 to 0.4 yielded a linear increase in the shear strength of samples in the range of 20 kPa to 70 kPa. The results of this paper were then validated accurately through some previous studies.

doi: 10.5829/ije.2024.37.05b.19

Graphical Abstract



*Corresponding Author Email: bolouri@um.ac.ir (J. Bolouri Bazaz)

Please cite this article as: Abdollahi M, Bolouri Bazaz J, Akhtarpour A. Cyclic and Monotonic Behavior of Non-plastic Silts with the Presence of Initial Static Shear Stress Using Strain Energy Approach: A Case Study for a Tailings Dam. International Journal of Engineering, Transactions B: Applications. 2024;37(05):1036-49.

NOMENCLATURE

NOMENCLATURE		Greek Symbols	
q_s	Deviator stress at static loading	α	Initial static shear stress ratio
PT	Phase transformation point	τ_s	Initial static shear stress
CSL	Critical state line	σ'_{3c}	Effective confining pressure
r_u	Pore pressure ratio	σ_1	Maximum principal stress
CU	Consolidation-Undrained test (triaxial test)	σ_3	Minimum principal stress
W	Energy density	φ_{CSL}	Inclination of CSL, internal friction angle
W_{liq}	Capacity energy	τ_{PT}	Shear stresses at the phase transformation point
W/W_{liq}	Strain energy ratio		

1. INTRODUCTION

Tailings dam is one of the vital structures subjected to extensive failure under seismic loadings. It is crucial to note that tailings dam problems are not limited to design and construction. During the period of operation, tailings dams are known as a source of pollution alongside the human communities due to the production of a significant amount of contaminated materials (1). Consequently, destructive factors such as seepage, instability, and above all earthquake and dynamic loadings can lead to polluted surface and polluted groundwater. According to the USCOLD report (2), earthquake is the major cause of failure in tailing dams. This failure may occur if some parts of the tailings dam body is liquefied (2). Liquefaction is a challenging subject in geotechnical engineering problems, mostly in saturated loose sands and non-plastic silts. This phenomenon has been the cause of intensive failures in many earthquakes (3). The studies on the stability of tailings dams related to initial and final elevations of the dam crest under dynamic loading indicated that the liquefaction takes place for both dam body and impoundment, leading to the dam instability at the final elevation (4, 5). Some solutions such as vertical gravel column drains can reduce the liquefaction potential of a soft ground (6).

There are various techniques, including in-situ and experimental methods to assess the potential of liquefaction for several soils. For instance, based on spectral matching to a target spectrum, Hanindya et al. (7) developed an artificial time history of earthquake to study the liquefaction of a stratified ground and concluded that liquefaction potential reduces with increasing stiffness and depth of soil. Cone Penetration Test (CPT) results can also be employed to determine the liquefaction potential. For example, Latifi et al. (8) successfully analyzed the liquefaction problem for a zone in Morocco using CPT data. From a structural viewpoint, liquefaction potential of a ground can be assessed regarding physical characteristics of the subsurface structure determined based on two innovative geophysical approaches, including Rayleigh surface waves and electrical resistivities (9). In addition, the stress-based approach and strain energy-based method are two common experimental procedures in the literature (10-16). Among these methods, stress-based method has been more common among researchers for

liquefaction assessment (10, 17). In this procedure, the shear stress level, mean effective stress, and the number of cycles, are the critical parameters in estimating the liquefaction potential of cohesion-less soils. Although the stress-based approach is continually improved through recent attempts and increases in the number of studies on liquefaction, the uncertainty due to random loading needs to be addressed (18). However, the strain energy-based method is a relatively modern one to determine the silty soil liquefaction potential. Among those, the strain energy absorption model in soils for the liquefaction assessment is a new method recently considered by researchers (14, 16, 18, 19). In this method, the quantity of strain energy per unit volume dissipated in the deposit is utilized to assess the cyclic behavior of sands. In geomaterials subjected to cyclic loading, the cumulative area limited to the shear stress-strain loops indicates how strain energy density dissipates (14). In the past years, many researchers implied that the relationship between dissipated strain energy density and pore pressure buildup partially depends on the stress (14, 20, 21). The benefits of the strain energy method have led to additional research into the evaluation of potential liquefaction. The existence of a rational correlation among dissipated strain energy, residual pore pressure, and non-recoverable plastic deformation can be employed to develop energy-based pore pressure models through experimental results (14).

To assess the influences of initial static shear stress τ_s and mean effective stress p' , many researchers have conducted a wide range of laboratory tests on sands and silty sands (22-25) and FEM modeling for saturated sand (26). Furthermore, Iraj (27) analyzed finn-byrne model for liquefaction of quay and cantilevered retaining walls. Monotonic and cyclic loads are two conventional loading types in various geotechnical problems (28, 29). Previous attempts demonstrate that τ_s has a significant effect on shear resistance under monotonic and cyclic loading. For instance, it is concluded that the initial shear static ratio (α) is directly proportional to the number of cyclic shear stresses needed to initiate the liquefaction (30, 31). Besides, any increase or decrease in cyclic strength under initial static shear stress depends on the intensity of τ_s and the initial density of the soil (31). Under a given α , Hosono and Yoshimine (32) as well as Fakharian and Shabani (28) assessed the cyclic resistance of sand through numerous undrained cyclic triaxial tests. Their studies illustrated that the direction of the α has a

considerable impact on the cyclic strength of soil (28, 32).

The present research mainly investigates the influences of seismic loadings on pure silt related to the Sungun Copper tailings dam in Northwest Iran as a case study. This tailing dam was constructed using the upstream method. The evaluation of the liquefaction potential of saturated non-plastic silt is of particular importance. The monotonic and cyclic tests under different τ_s were performed using an automated cyclic triaxial system. A series of experimental tests was carried out using an automated cyclic triaxial system. The experiments on pure silt under monotonic loading revealed an unusual response for different densities from 25% to 80%. All tests demonstrated a relatively similar dilation rate, and their dilative trends were not remarkable for all ranges of densities from loose to dense conditions. In other words, there was no intensive strain hardening in stress-strain diagrams, even for very dense silty soils. For the cyclic condition, tests were conducted on silts using the strain-energy method. The experimental results indicated dramatic changes in the dissipated strain energy required for the liquefaction by changing the σ'_{3c} and τ_s .

2. MATERIAL AND SAMPLE PREPARATION

Sungun copper mine is one of the open pit mines situated in the northwestern region ($43^\circ 46'$ East and $38^\circ 42'$ North) of Iran, close to the Aras River (Figure 1). Metal minerals are widely present in the geological features of the Aras watershed. Sungun copper mine is very important in terms of industry and geological formations in the mentioned area. This mine started its activity in 1990 and is known as a productive reserve of almost 800 million tons of 0.67-grade copper ore. Hence, a minimum of 380 million tons of copper waste can be produced during 25 years (33).

From a geological viewpoint, the studied region is situated in the Oligocene volcanic area. It includes calc-



Figure 1. Sungun porphyry copper mine located in Iran

alkaline volcanic minerals, mainly trachy-andesite, andesite, and dacite containing basaltic lava (34). Sungun porphyry copper deposits are found in trachyandesite rocks that contain cool silver-colored porphyry latite of medium to high resistance and medium to severe weathering. The color of the areas influenced by the penetration of underground water changes to brown in some locations. Moreover, small amounts of sulfide minerals containing chalcopyrite and pyrite are observed in the lower depths. The material used in this study is non-plastic silt supplied from Sungun Porphyry copper mine with the characteristics given in Table 1. The simplified lithology map of Sungun copper mine is shown in Figure 2. The X-ray diffraction (XRD) test that was carried out on the materials as plotted in Figure 3. The results of XRD analysis include compound name, percent of each mineral, and chemical formula.

The distribution of particle size is presented in Figure 4. The magnified photos (SEM) of the silt sample are illustrated in Figure 5 with two different magnifications ($20 \mu\text{m}$ & $10 \mu\text{m}$). The magnified photos show angular particle shapes, and the surface of the particles looks relatively smooth.

Experiments were carried out on samples with diameter and height of 50 mm and 100 mm, respectively, using a monotonic/cyclic triaxial device. The moist tamping method is employed to prepare the samples (Figure 6). In moist tamping, the sand with 12% moist was tamped in 5 layers to achieve the desired void ratio.

TABLE 1. Characteristics of the Sungun copper tailings samples

(a) Quantitative X-ray diffraction (XRD) analysis		
Compound	Percent (%) (By atomic weight)	Chemical formula
Silicate	43.9	Si O ₂
Illite	34.3	Al ₂ H ₂ K O ₁₂ Si ₄
Kaolinite	8.7	Al ₂ H ₄ O ₉ Si ₂
Iron (II) duo-disulfide Marcasite	6.1	Fe S ₂
Quartz	1.6	O ₂ Si
Unidentified peak area		
(b) Geotechnical properties		
Parameter	Symbol	Value
Specific gravity	G _s	2.70-2.73
Internal friction angle (deg)	ϕ'	11.2-36.7
Liquid limit	LL	23.6-25.3
Minimum dry unit weight (kN/m ³)	$\gamma_{d(\text{min})}$	12.36
Maximum dry unit weight (kN/m ³)	$\gamma_{d(\text{max})}$	15.46

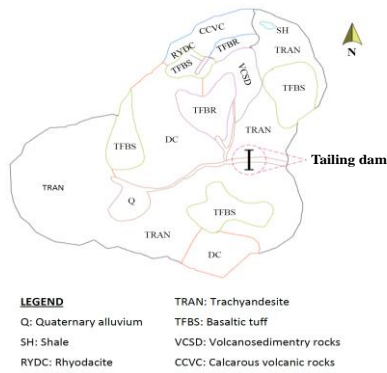


Figure 2. Simplified lithology map of Songgun copper mine

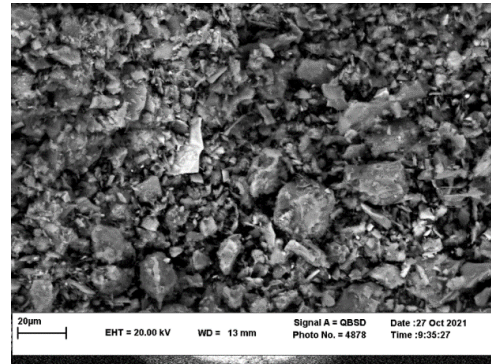


Figure 5. Microscopic scanning of pure silt (a) scale 20 µm (b) 10 µm

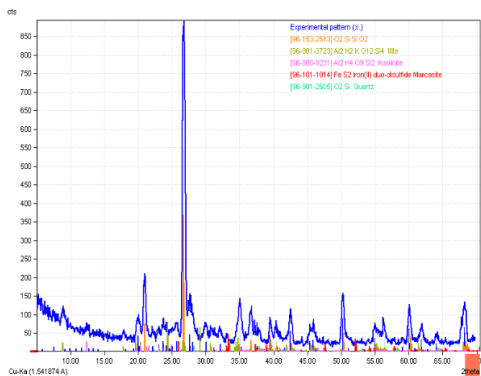


Figure 3. Experimental pattern of Sungun silt components

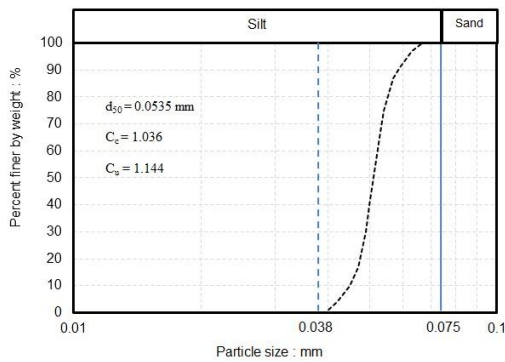
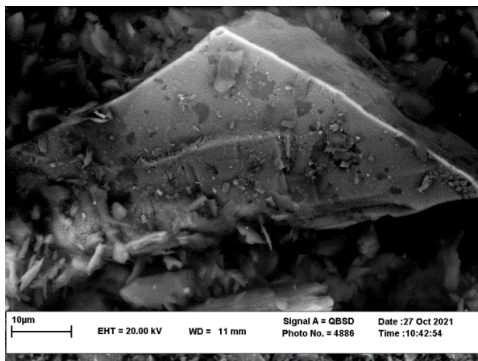


Figure 4. Particle size distribution



(a)



Figure 6. Sample preparation in Triaxial device

The weight and height of each layer were measured separately depending on the number of the layers using the moist tamping method suggested by Ladd (35). Carbon dioxide was initially circulated for 60 min, followed by passing de-aired water equivalent to double of sample volume, to ensure better saturation. By applying a 10 kPa cell pressure, sample disturbance during de-aired water circulation can be prevented. Fully saturated samples were achieved with Skempton's B-

values exceeding 0.95. After saturation, consolidation of the whole samples under the desired σ'_{3c} was performed. The duration for consolidation often took 2 h for pure silt samples.

3. TEST PROGRAM

In the current study, the critical state parameters and liquefaction potential of silty sand are evaluated through a wide range of laboratory monotonic and cyclic experiments. All tests were performed on samples with initial densities of 25, 45, 60, and 80%.

As the first phase, a set of monotonic tests was planned to determine the soil mechanical parameters as well as the critical state line (CSL). For all tests, three consolidation stress paths, including one isotropic and two anisotropic paths ($\alpha = 0, 0.2, \text{ and } 0.4$), were chosen (see Eq.1). All monotonic tests (see Table 2) were carried out with three different effective mean stresses p' of 50, 100, and 150 kPa along with one test under p' of 400 kPa (only for comparison) to investigate isotropic and anisotropic consolidation. The values for α were selected as 0 (i.e., isotropic condition), 0.2, and 0.4, (i.e., anisotropic condition). The isotropic and anisotropic

stages of drained loading are applied respectively to meet the final magnitude of τ_s related to the consolidation part. After consolidation, monotonic tests were initiated by applying deviatoric stress and terminated when reaching 20 percent of shear strain.

In the second phase, nine cyclic tests (see Table 2) were conducted to assess the liquefaction potential of pure silt samples. The investigation into the influences of τ_s and σ'_{3c} on the cyclic behavior is also intended. All cyclic experiments were conducted by loading the samples under strain-controlled conditions to estimate capacity energy W_{liq} and residual pore pressure. Table 2 demonstrates the test programs, including p' , D_r , and α for monotonic and cyclic conditions.

4. MONOTONIC TEST RESULTS

4.1. Influences of D_r and Σ'_{3c} The initial tests were conducted on non-plastic silt at 25, 45, 60, and 80% relative densities to assess the soil behavior. Saturated and consolidated samples were subjected to strain-controlled undrained shearing at a 0.05 mm/min deformation rate. Figures. 7a, 7b, and 7c demonstrate τ - γ , u_e - γ diagrams and the effective stress paths,

TABLE 2. Summary of triaxial tests schedule performed in the present research

Test Name	Confining pressure (kPa)	Relative final density (%)	Initial shear stress ratio (α)	Loading type	Shear strain amplitude (%)
T100-25-0m	100	25	0	monotonic	20
T100-45-0m	100	45	0	monotonic	20
T100-60-0m	100	60	0	monotonic	20
T100-80-0m	100	80	0	monotonic	20
T50-50-0m	50	45-50	0	monotonic	20
T100-50-0m	100	45-50	0	monotonic	20
T150-50-0m	150	45-50	0	monotonic	20
T400-50-0m	400	45-50	0	monotonic	20
T50-50-0.2m	50	45-50	0.2	monotonic	20
T100-50-0.2m	100	45-50	0.2	monotonic	20
T150-50-0.2m	150	45-50	0.2	monotonic	20
T50-50-0.4m	50	45-50	0.4	monotonic	20
T100-50-0.4m	100	45-50	0.4	monotonic	20
T150-50-0.4m	150	45-50	0.4	monotonic	20
T50-50-0c	50	45-50	0	cyclic	0.75
T100-50-0c	100	45-50	0	cyclic	0.75
T150-50-0c	150	45-50	0	cyclic	0.75
T50-50-0.2c	50	45-50	0.2	cyclic	0.75
T100-50-0.2c	100	45-50	0.2	cyclic	0.75
T150-50-0.2c	150	45-50	0.2	cyclic	0.75
T50-50-0.4c	50	45-50	0.4	cyclic	0.75

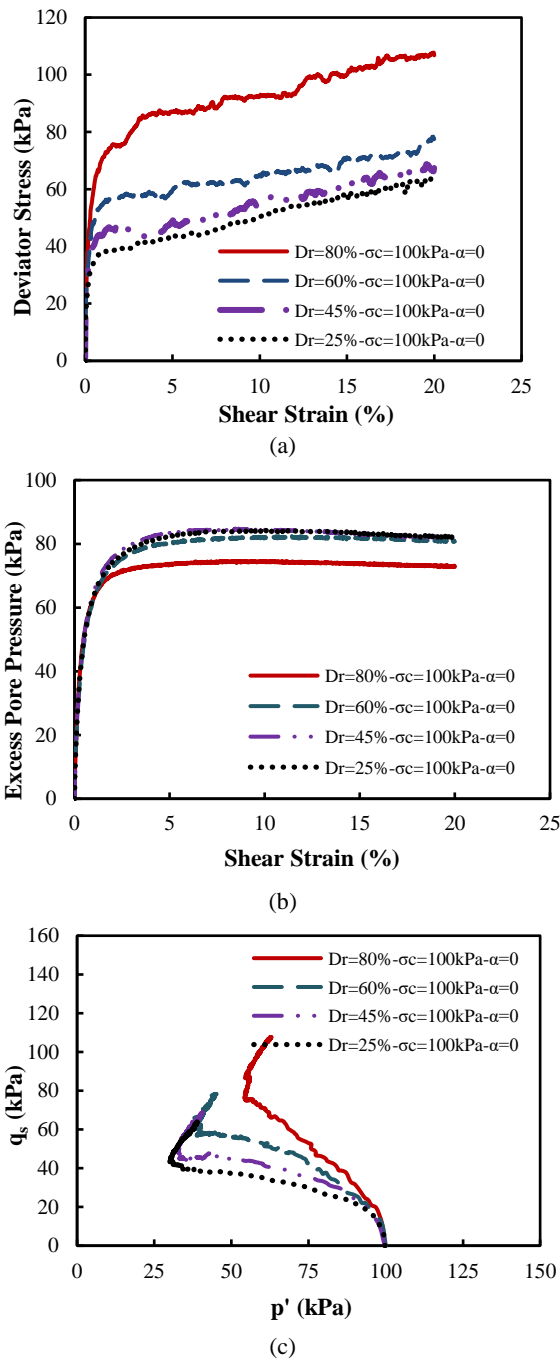


Figure 7. Monotonic behavior of pure silt for loose to dense samples - current study a) q_s - γ b) u_e - γ c) Stress paths

respectively. Clearly, all samples illustrate a slight strain-hardening behavior. In other words, samples are moderately dilated when axial strain is enhanced, even for the loosest conditions.

For medium to dense conditions, it is usually expected an intensive dilative response for non-cohesive soils, while in this study, a slight dilation was observed

even at 80% density. Karim and Alam (36) observed a similar response for loose and dense non-plastic silts. They compared the behavior of pure silt, clean sand, and different mixtures of sand and silt extensively. Figure 8 shows a highly dilated response of sand compared with a shallow dilative behavior of silt in the same density of 78% (36).

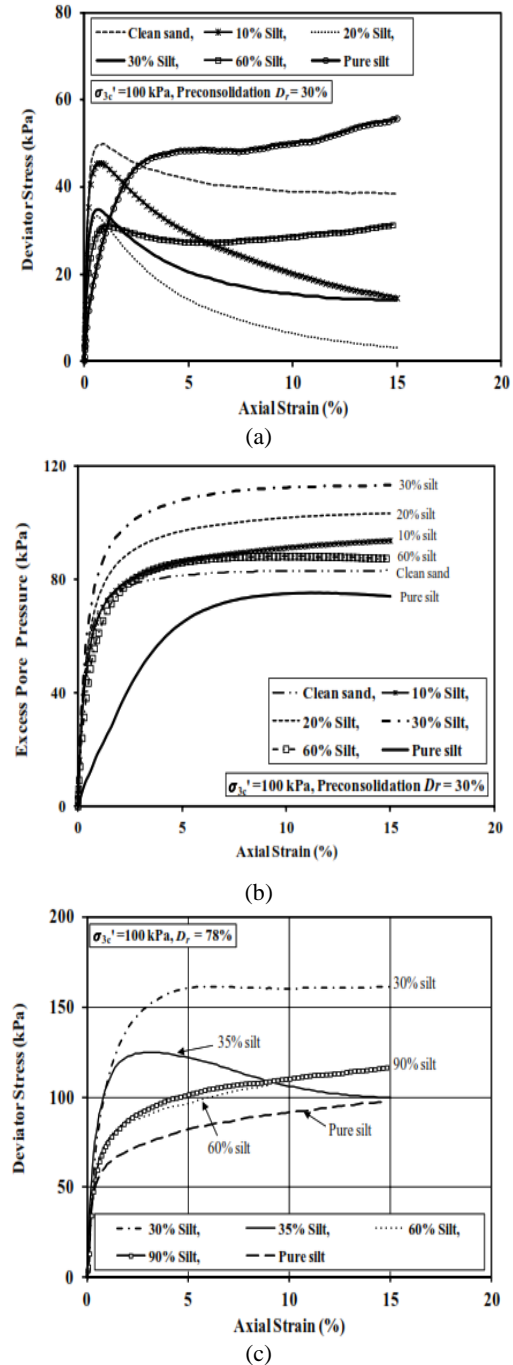


Figure 8. a) q_s and u_e versus axial strain ϵ for 30% density b) q_s versus ϵ for 78% density (36)

Similarly, the results in the present study support the observations mentioned above by Karim and Alam (36). This behavior of slight dilation in silty materials seemingly results from the small size of grains and their relatively smooth surface (as shown in Figure 5b). During current tests, applying a mean effective confining pressure of 100 kPa, increased the initial densities of samples by 25% to 30% as compared to the initial condition, depending on their first density. Several experiments were conducted with four σ'_{3c} values including 50 kPa, 100 kPa, 150 kPa, and 400 kPa to investigate the confining pressure impact on loose non-plastic silts. By increasing the σ'_{3c} , soils tend to show more contractive behavior. Thus, σ'_{3c} was increased up to 400 kPa so that contractive behavior was observed. The sample was prepared with 5% density initially and after applying $\sigma'_{3c} = 400$ kPa, the final density before applying shear loads reached 50%. Preparing the sample with negative density to achieve a looser sample (after consolidation) was impossible in this particular silt. As seen in Figure 9, irrespective of σ'_{3c} magnitude, all samples demonstrated contractive behavior (i.e., strain-softening) initially, and then followed by dilative behavior (i.e., strain-hardening) with increasing the axial strain even at high σ'_{3c} levels. This transition happened after reaching the phase transformation (PT) point. It was shown that at PT point, contractive behavior changes into dilative behavior while u_e experiences its maximum pressure within the test (37). Moreover, any complete loose state response or even flow liquefaction point (peak point) was not observed through the experiments.

4. 2. Influence of α In many geotechnical engineering, there are several situations in which the soil stratum is subjected to the in-situ τ_s . To examine this issue, the effect of τ_s in the sloping parts of the dam should be assessed. For this purpose, the adequate mean stresses of 50, 100, and 150 kPa were applied to samples to be isotropically consolidated first. Afterward, by applying τ_s to the sample in a drained condition, it was

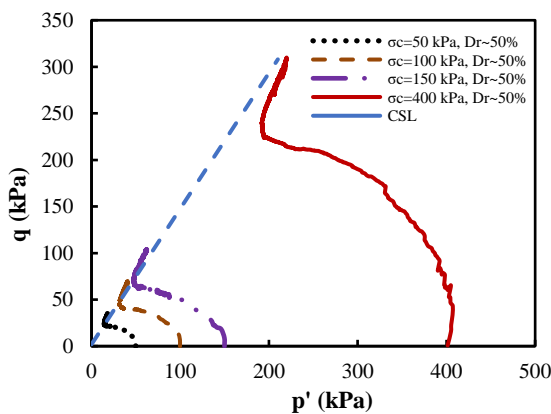


Figure 9. Influence of σ'_{3c} on Sungun silt behavior

consolidated anisotropically as shown in Figure 10. The initial static shear stress ratio is expressed as:

$$\alpha = \frac{\tau_s}{\sigma'_{3c}} \tag{1}$$

$$\tau_s = \frac{q_s}{2} = \frac{\sigma_1 - \sigma_3}{2} \tag{2}$$

Figure 11 illustrates three tests results considering three values for the α under a given mean effective stress of 150 kPa when $\alpha = 0, 0.2, \text{ and } 0.4$. Based on input data, the critical state line (CSL) and the phase transformation line (PTL) were drawn in this figure as well.

The friction angle of granular soils in the steady state is called the critical state friction angle of the soil and is indicated by ϕ_{CSL} . This friction angle is widely applied as a very important feature in geotechnical projects as well as in various behavioral models. The critical state line in the q - p' plane is reflected well by a straight line passing through the origin:

$$q = M_{CSL} \cdot p' \tag{3}$$

where M_{cs} is a constant equal to the stress ratio at critical state. The critical state friction angle ϕ_{CSL} in triaxial compression conditions can be obtained from the stress ratio at critical state using Equation 4:

$$\sin \phi_{CSL} = \frac{3M_{CSL}}{6+M_{CSL}} \tag{4}$$

The inclination of CSL (i.e., internal friction angle ϕ_{CSL}) was equal to 37° . Besides, it is worth noting that all ultimate points stand on a unique CSL regardless of the initial anisotropic condition. In other words, the loci of critical state lines are not governed by the τ_s . These results follow the findings concluded in a study based on the Discrete Element Method by Zhao et al. (38) in which no correlation between the mean effective stress and CSL was reported. By increasing the α , the effective stress state approaches the CSL (39). Thus, the strain-softening

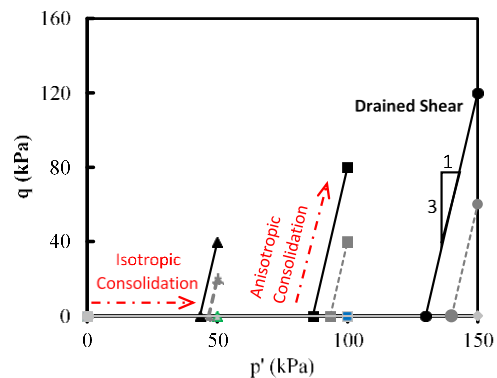
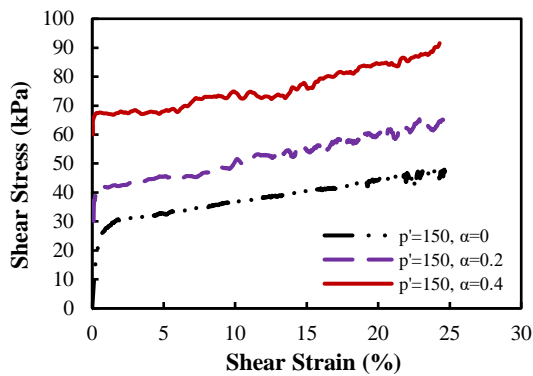
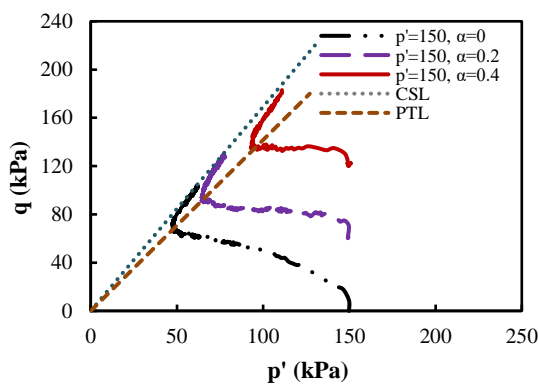


Figure 10. Drained stress path before monotonic and cyclic loadings



(a)



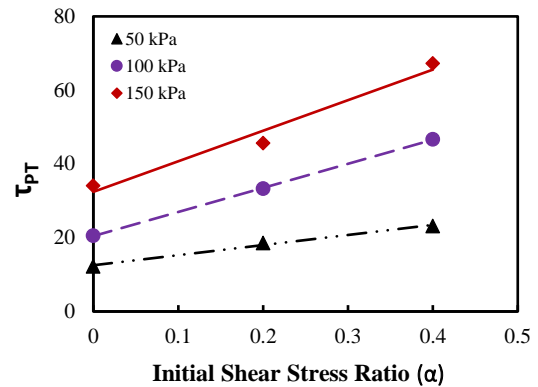
(b)

Figure 11. Influence of τ_s on Sungun silt response, a) τ - γ , b) Stress paths

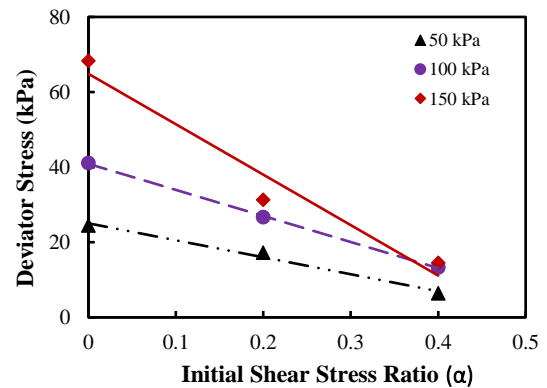
deformations might occur with a small trigger. Monotonic test results demonstrated in Figure 11 followed this trend. The stress path diagrams of 3 undrained tests for three values of the α parameter, including 0, 0.2, and 0.4 were presented in Figure 11. While a sample with no initial shear stress ratio (i.e., $\alpha = 0$) shows no peak point and subsequently strain-hardening behavior was seen in all phases of the test, samples under the τ_s of 0.4 experienced a partial strain-softening behavior and indicated a peak point before reaching to the phase transformation (PT) point.

From Figure 12, the increase of α from 0 to 0.4 will lead to a linear increase in the shear strength of samples. Therefore, the τ will experience a higher level of strength through the compressive loading. These findings have been shown in Figure 12a for shear stresses at phase transformation point (τ_{PT}) under the various amounts of σ'_{3c} as well as different amounts of τ_s values. As seen in this figure, an increase in both σ'_{3c} and τ_s changes the amount of phase transformation point and, consequently the shear stress level at PT (τ_{PT}). This behavior is in appliance with previous studies by Rasouli et al. (40).

Another parameter assessed in the current study was the deviator stress applied to the soil from the end of consolidation and the beginning of loading until the



(a)



(b)

Figure 12. Influence of τ_s on a) shear stress at PT, b) Required Deviator Stress at PT after anisotropic consolidation

phase transformation point. Variations of deviator stress versus the α value at 50, 100, and 150 kPa mean effective stresses are presented in Figure 12. Considering the test results for different values of α , the deviator stress required to reach the PT point is diminished with rising the intensity of τ_s . This decline is interpreted by the state of stresses associated with the critical state line. When the τ_s is exerted on the sample, the travel distance to the CSL decreases, and consequently, less shear loading is required for failure. It is evident that for the highest τ_s , the sample experiences a slight increase in deviator stress to achieve the phase transformation point. Moreover, as shown in Figure 12b, a more significant amount of mean effective stress will increase the shear stress level.

5. CYCLIC TEST RESULTS

Numerous laboratory experiments were carried out using a cyclic triaxial device to investigate the cyclic behavior of the Sungun non-plastic silt. The liquefaction resistance and pore pressure development were determined based on the strain energy approach using the results of various tests conducted with the strain control state. In this approach, the quantity of strain energy per unit volume

dissipated in the deposit (also called unit energy and energy density (41)) is utilized to assess the cyclic response of silt (14). The main parameters of the strain energy approach include energy density dissipated instantaneously (W), capacity energy (W_{liq}) and strain energy ratio (W/W_{liq}) (14, 18). It should be noted that in addition to soil and porous media, the approach is effectively applied to investigate the cyclic behavior of structural elements (e.g., steel plates (42); reinforced concrete (43); alloy beams (44)) under earthquake conditions. The achievement of a pore pressure ratio (r_u) of 1 is assumed an appropriate criterion for liquefaction occurrence. The tests can provide the clarification on how τ_s and σ'_{3c} affect the liquefaction response.

As stated in Section 2, the moist tamping method was used to prepare samples considering the under-compaction coefficient. The initial density of prepared samples was selected based on their σ'_{3c} as such final density after consolidation reached the relatively same amount of 45%. Undrained (CU) tests were performed on loose samples with three initial relative densities of 10%, 20%, and 25% under three σ'_{3c} values including 50 kPa, 100 kPa, and 150 kPa, respectively. While the consolidation of 50 kPa, 100 kPa, and 150 kPa were applied to the sample, the relative density of this non-plastic silt was somewhat increased by 20, 25, and 30%, respectively. An increase in density of the Sungun silt due to the application of σ'_{3c} seems to be more intense than what sand experienced during the consolidation process under the same conditions as reported by Karim and Alam (36).

5. 1. Influence of γ All cyclic tests were performed considering the shear amplitude of 0.75% and frequency of 0.3 Hz. Figure 13 shows loops of $u_e-\gamma$ and $\tau-\gamma$ for a cyclic test with a 100 kPa σ'_{3c} and 50 % density. It is evident that the most energy dissipation takes place at the first cycle having the highest stiffness. Besides, the maximum magnitude of u_e , the most reduction in shear modulus and stiffness, happened at the first cycle.

Variations of τ , γ , r_u , and W with the number of cycles N , are illustrated in Figures 14a to 14d, respectively. It is shown that applying the cyclic strain-control loading raises the u_e instantly, leading to a decrease in the shear stress capacity. In addition, W is monotonically increased with time until soil failure.

5. 2. Influences of τ_s and σ'_{3c} In this section, the impacts of in-situ τ_s and σ'_{3c} derived at sloping parts of the dam on pore pressure buildup, energy density and consequently, liquefaction potential of the current tailings dam are discussed. To this aim, a series of comparisons is provided to assess the role of τ_s .

First, variations of u_e versus W for the p' of 50 kPa, 100 kPa, and 150 kPa and three values for α , including 0, 0.2, and 0.4 were plotted in Figure 15. Clearly, there is a rational correlation between dissipated energy density

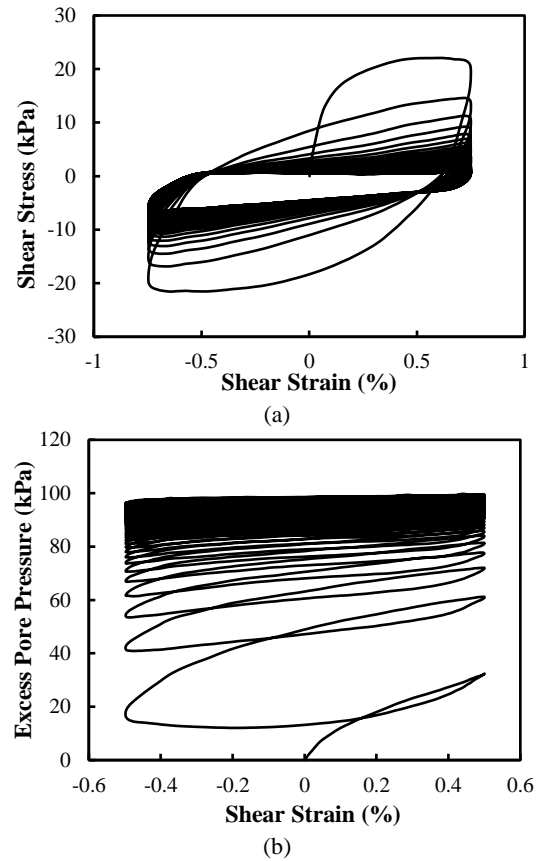
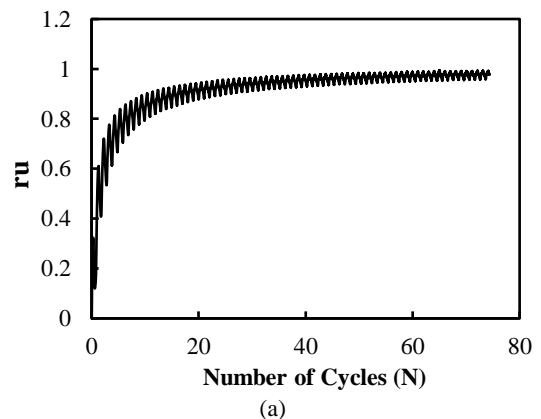
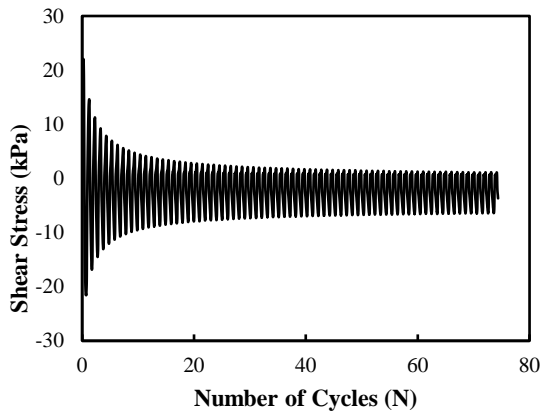


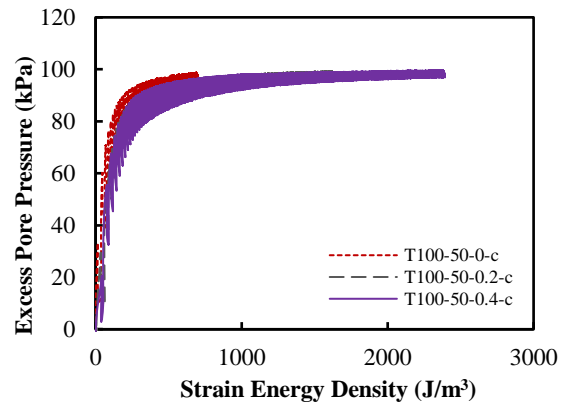
Figure 13. Results of cyclic tests in terms of the shear strain for Sungun silt when $D_r = 50\%$ and $\sigma'_{3c} = 100$ kPa

and pore pressure buildup in different conditions. The test results also implies that a considerable energy density is required for higher values of mean effective stress and α . In other words, the energy density necessitated at liquefaction time increases with p' and τ_s applied to the sample. As a result, mean effective stress and α have a significant impact on the Sungun pure silt from a viewpoint of liquefaction resistance. All tests were plotted until the corresponding liquefaction cycle number.

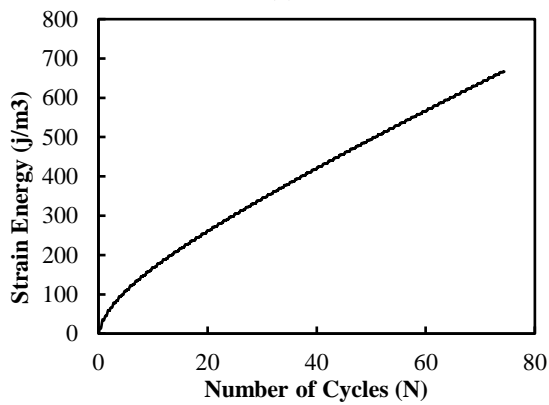




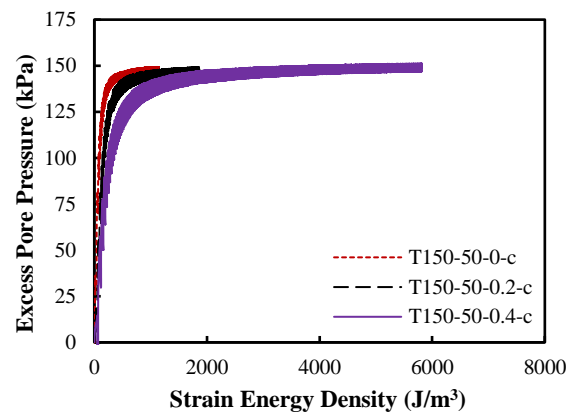
(b)



(b)



(c)



(c)

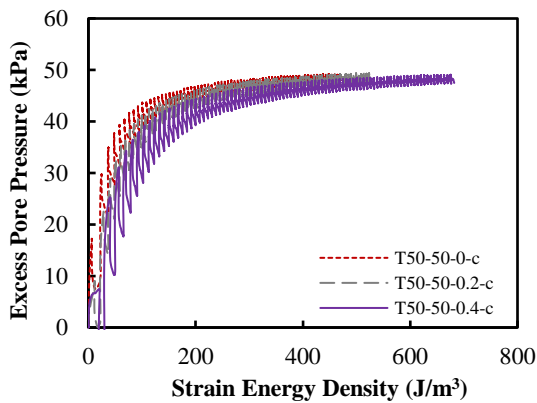
Figure 14. Results of cyclic tests in terms of the number of cycles for Sungun pure silt when $D_r=50\%$ and $\sigma_c=100$ kPa

Figure 15. Variations of u_e versus W at three σ'_{3c} values of 50,100 & 150 kPa, and α of 0, 0.2 & 0.4 on Sungun silts

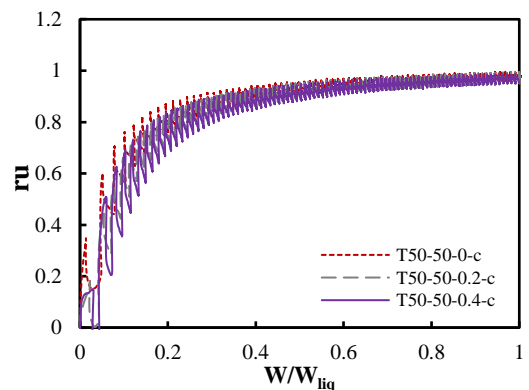
Figure 16 compares the impact of τ_s for three values of σ'_{3c} in terms of r_u-W/W_{liq} . As can be seen, there is no essential difference in the trends and magnitudes of all graphs. In other words, variation in τ_s reflects just a negligible impact on the r_u-W/W_{liq} relationship. This trend for the Sungun samples was roughly similar to that for Toyoura sand as concluded by Jafarian et al. (14). The similarity of r_u-W/W_{liq} curves could be a reflection of the

normalization of strain energy density (W) by capacity energy (W_{liq}). In other words, τ_s affects both strain energy and capacity energy simultaneously, and consequently, its influence is reduced essentially.

To indicate the impact of initial mean effective stress and τ_s (or adequate confining pressure σ'_{3c}) clearly, a set of diagrams compared the capacity energy of sample at the liquefaction time. As presented in Figure 17, the



(a)



(a)

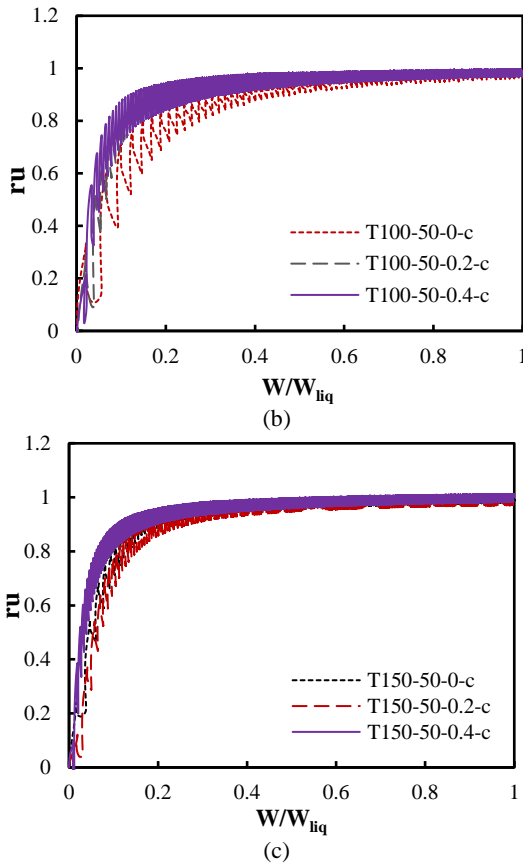


Figure 16. Variation of r_u against W/W_{liq} , at three σ'_{3c} values of 50,100 & 150 kPa, and α of 0, 0.2 & 0.4 on Sungu silt

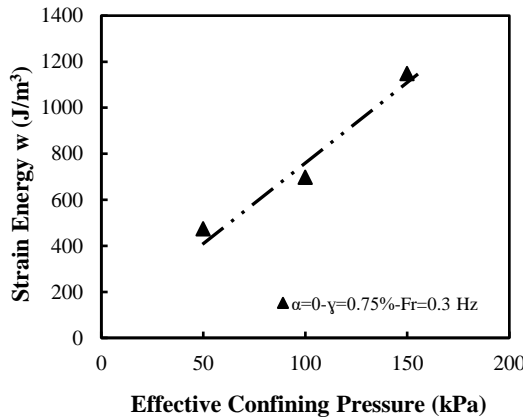


Figure 17. Variation of W required for liquefaction against σ'_{3c} in the current study

effect of σ'_{3c} is entirely evident in the amount of W . The more σ'_{3c} is applied, the further the level of W is gained. Thus, while two samples have a relatively similar density, the firmer one (with higher σ'_{3c}) requires greater energy density to be liquefied. This trend is in good agreement with that reported in some previous studies (14, 16, 30, 45) under both experimental and numerical modelings as shown in Figure 18.

Figure 19a presents three lines corresponding to three amounts considered for α . It should be noted that the rate of dissipated energy density dramatically increases with the α . For instance, the amount of energy density rises from 474 J/m³ to 1147.4 J/m³ for $\alpha = 0$, while it encounters a more intense increase from 682 J/m³ to 5839 J/m³ for $\alpha = 0.4$. Furthermore, Figure 19b illustrates the variation of dissipated W versus α . It is observed that the required energy for liquefaction rises with an increase in the α value. However, the increasing rate of energy

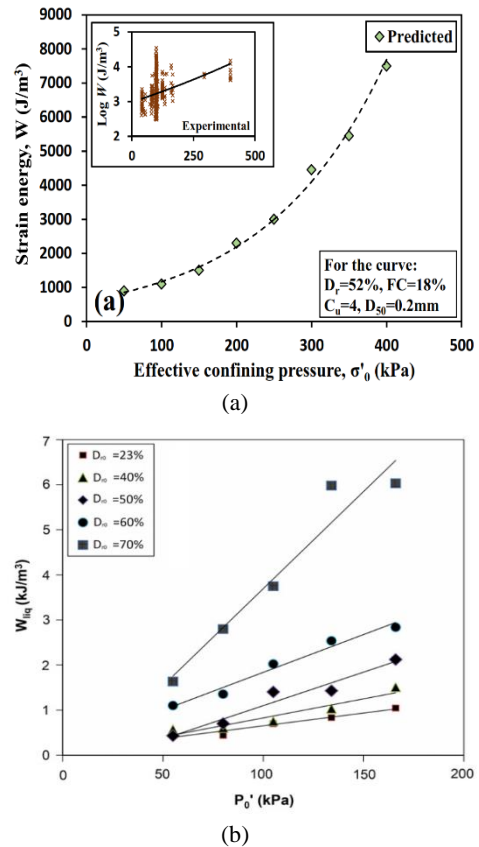
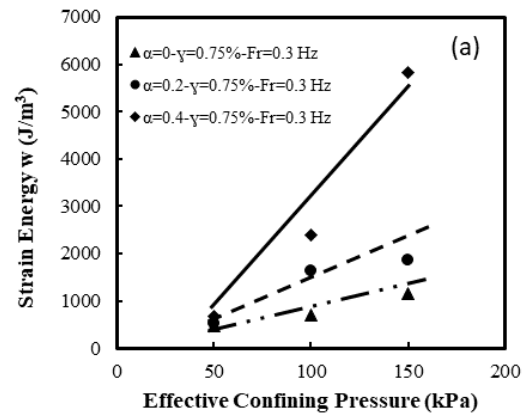


Figure 18. Variations of W against a) σ'_0 , Javdian (45), b) σ'_{3c} , Jafarian et al. (14)



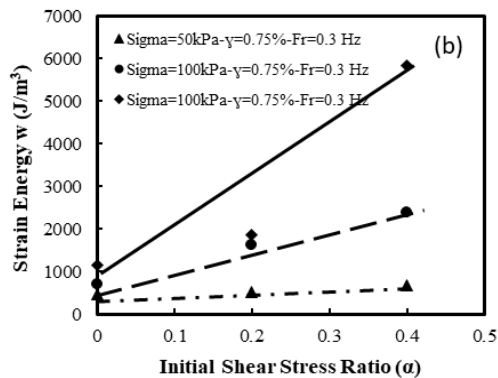


Figure 19. Variations of W against a) σ'_{3c} , b) α for pure silt in the current study

density is quite different for various σ'_{3c} . For example, under the lowest confining pressure (i.e., 50 kPa), when the τ_s was increased from 0 to 0.4, the growth of energy density was almost 204 J/m³, while increasing the σ'_{3c} up to 150 kPa, raised the growth of energy density to 4690 J/m³. This means that τ_s rather affects the energy dissipated for liquefaction, however, the increment rate strongly depends on the σ'_{3c} intensity.

6. CONCLUSION

The strain energy approach conventionally captures the simultaneous effects of stress and strain influence to assess the liquefaction phenomenon for clean sands or silty sand. Pure silt is found as a main part of tailings material extracted from the Sungun copper mine, which is susceptible to liquefaction. In this research, the liquefaction potential of silt-sized copper waste deposits behind the tailings dam was evaluated using the strain energy method. It considers the cyclic response of silt based on the quantity of strain energy per unit volume dissipated in the deposit. Several triaxial tests were conducted under different conditions to investigate the influences of effective mean stress p' (or confining pressure σ'_{3c}) and initial shear stress τ_s on the behavior of particular silts related to the Sungun copper tailings through monotonic and dynamic loadings.

Based on monotonic and cyclic test results obtained in the current research, the key findings may be drawn as follows:

1. Monotonic test results revealed a low tendency for a dilative response even at the dense states of Sungun silt. Density change after consolidation was moderately high even under low σ'_{3c} (e.g., 20% for 50 kPa), in contrast with that for granular materials reported in previous studies. The slight dilation in the dense samples stemming from the negligible reduction of pore pressure could attributed to the extremely small grains and the low roughness of the Sungun silt particles.

2. An increase of τ_s for monotonic tests led to a higher resistance in terms of shear stress.

3. A unique critical state line (CSL) was attained under different amounts of p' and α .

4. As the τ_s increased, the locus of shear stress approached the critical state line, and the deviator stress level required to reach the CSL was reduced.

5. Cyclic and monotonic test results showed the same trends. The energy density required for the liquefaction of Sungun pure silt was completely dependent upon σ'_{3c} and α . The capacity energy monotonically increased with σ'_{3c} . A sample with a higher D_r needed a greater energy density for the liquefaction. The cumulative energy density for liquefaction was directly proportional to τ_s .

6. The growth rate in capacity energy at higher σ'_{3c} was dramatically increased with τ_s . It rose sharply with any increase of σ'_{3c} at higher τ_s levels.

7. REFERENCES

1. Jafarzadeh Marandi M, Ghiasi V, Badv K. Numerical Evaluation of Two-dimensional Multi-layer Cover System to Regulate Acid Mine Drainage of Tailing Dams. *International Journal of Engineering, Transactions A: Basics*. 2023;36(10):1839-56. [10.5829/ije.2023.36.10a.10](https://doi.org/10.5829/ije.2023.36.10a.10)
2. USCOLD TDI. US Committee on Large Dams (USCOLD). Denver, Colorado. 1994.
3. Koketsu K, Miyake H. A seismological overview of long-period ground motion. *Journal of Seismology*. 2008;12(2):133-43. <https://doi.org/10.1007/s10950-007-9080-0>
4. Xu B, Wang Y. Stability analysis of the Lingshan gold mine tailings dam under conditions of a raised dam height. *Bulletin of Engineering Geology and the Environment*. 2015;74(1):151-61. <https://doi.org/10.1007/s10064-014-0602-z>
5. Naeini M, Akhtarpoor A. Numerical analysis of seismic stability of a high centerline tailings dam. *Soil Dynamics and Earthquake Engineering*. 2018;107:179-94. <https://doi.org/DOI:10.1016/j.soildyn.2018.01.019>
6. Hamed Sangari A, Marandi SM. Laboratory Studies on the Effect of Vertical Gravel Column Drains on Liquefaction Potential. *International Journal of Engineering*. 2011;24(3):209-26. https://www.ije.ir/article_71914_b325c15a6d012b938b1c9470f3233b11.pdf
7. Hanindya KA, Makrup L, Widodo, Paulus R. Deterministic Seismic Hazard Analysis to Determine Liquefaction Potential Due to Earthquake. *Civil Engineering Journal*. 2023;9(5):1203-16. [10.28991/CEJ-2023-09-05-012](https://doi.org/10.28991/CEJ-2023-09-05-012)
8. Latifi FE, Baba K, Ardouz G, Bouanani LE. Evaluation of Liquefaction Potential based on Cone Penetration Test (CPT) and Semi-empirical Methods. *Civil Engineering Journal*. 2023;9(2):423-36. [10.28991/CEJ-2023-09-02-013](https://doi.org/10.28991/CEJ-2023-09-02-013)
9. Özcan Çakır, Coşkun N. Dispersion of Rayleigh Surface Waves and Electrical Resistivities Utilized to Invert Near Surface Structural Heterogeneities. *Journal of Human, Earth, and Future*. 2022;3(1):1-16. [10.28991/HEF-2022-03-01-01](https://doi.org/10.28991/HEF-2022-03-01-01)
10. Seed HB, Idriss IM. Simplified procedure for evaluating soil liquefaction potential. *Journal of the Soil Mechanics and Foundations division*. 1971;97(9):1249-73. <https://doi.org/10.1061/JSFEAQ.0001662>

11. Ishihara K. Liquefaction and flow failure during earthquakes. *Geotechnique*. 1993;43(3):351-451. <https://doi.org/10.1680/geot.1993.43.3.351>
12. Vaid Y, Sivathayalan S. Static and cyclic liquefaction potential of Fraser Delta sand in simple shear and triaxial tests. *Canadian Geotechnical Journal*. 1996;33(2):281-9. <https://doi.org/10.1139/t96-007>
13. Nemat-Nasser S, Shokoh A. A unified approach to densification and liquefaction of cohesionless sand in cyclic shearing. *Canadian Geotechnical Journal*. 1979;16(4):659-78. <https://doi.org/10.1139/t79-076>
14. Jafarian Y, Towhata I, Baziar M, Noorzad A, Bahmanpour A. Strain energy based evaluation of liquefaction and residual pore water pressure in sands using cyclic torsional shear experiments. *Soil Dynamics and Earthquake Engineering*. 2012;35:13-28. <https://doi.org/10.1016/j.soildyn.2011.11.006>
15. Chen Y, Hsieh S, Chen J-W, Shih C. Energy-based probabilistic evaluation of soil liquefaction. *Soil Dynamics and Earthquake Engineering*. 2005;25(1):55-68. <https://doi.org/10.1016/j.soildyn.2004.07.002>
16. Baziar M, Sharafi H. Assessment of silty sand liquefaction potential using hollow torsional tests—An energy approach. *Soil Dynamics and Earthquake Engineering*. 2011;31(7):857-65. <https://doi.org/10.1016/j.soildyn.2010.12.014>
17. Whitman RV. Resistance of soil to liquefaction and settlement. *Soils and Foundations*. 1971;11(4):59-68. https://doi.org/10.3208/sandf1960.11.4_59
18. Baziar M, Jafarian Y. Assessment of liquefaction triggering using strain energy concept and ANN model: capacity energy. *Soil Dynamics and Earthquake Engineering*. 2007;27(12):1056-72. <https://doi.org/10.1016/j.soildyn.2007.03.007>
19. Zhang W, Goh AT, Zhang Y, Chen Y, Xiao Y. Assessment of soil liquefaction based on capacity energy concept and multivariate adaptive regression splines. *Engineering Geology*. 2015;188:29-37. <https://doi.org/10.1016/j.enggeo.2015.01.009>
20. Liang L. Development of an energy method for evaluating the liquefaction potential of a soil deposit: Case Western Reserve University; 1995.
21. Towhata I, Ishihara K. Shear work and pore water pressure in undrained shear. *Soils and foundations*. 1985;25(3):73-84. https://doi.org/10.3208/sandf1972.25.3_73
22. Boulanger RW, Seed RB. Liquefaction of sand under bidirectional monotonic and cyclic loading. *Journal of geotechnical engineering*. 1995;121(12):870-8. [https://doi.org/10.1061/\(ASCE\)0733-9410\(1995\)121:12\(870](https://doi.org/10.1061/(ASCE)0733-9410(1995)121:12(870)
23. Hosono Y, Yoshimine M. Effects of anisotropic consolidation and initial shear load on liquefaction resistance of sand in simple shear condition. *Geotechnical engineering for disaster mitigation and rehabilitation*. 2008:352-8. https://doi.org/10.1007/978-3-540-79846-0_37
24. Wei X, Yang J. Cyclic behavior and liquefaction resistance of silty sands with presence of initial static shear stress. *Soil Dynamics and Earthquake Engineering*. 2019;122:274-89. <https://doi.org/10.1016/j.soildyn.2018.11.029>
25. Pan K, Yang Z. Effects of initial static shear on cyclic resistance and pore pressure generation of saturated sand. *Acta Geotechnica*. 2018;13(2):473-87. <https://doi.org/10.1007/s11440-017-0614-5>
26. Marandi SM, Rasti AR. Parametric Study of the Covering Soil of Tunnels Constructed in Liquefiable Soil. *International Journal of Engineering*. 2012;25(4):333-46. <https://doi.org/10.5829/idosi.ije.2012.25.04a.05>
27. Iraj A. Evaluating Finn-Byrne Model in Liquefaction Analysis of Quay Wall and Cantilevered Retaining Wall Models. *International Journal of Engineering*. 2023;36(6):1075-91. <https://doi.org/10.5829/ije.2023.36.06c.06>
28. Fakharian K, Shabani F. Monotonic and cyclic experimental results of Chamkhaleh SAND in southern Caspian Sea. The Twenty-first International Offshore and Polar Engineering Conference. 2011. https://www.researchgate.net/publication/370124695_Monotonic_and_Cyclic_Experimental_Results_of_Chamkhaleh_Sand_in_Southern_Caspian_Sea
29. Hoseini MH, Noorzad A, Zamanian M. Physical Modelling of a Strip Footing on a Geosynthetic Reinforced Soil Wall Containing Tire Shred Subjected to Monotonic and Cyclic Loading. *International Journal of Engineering*. 2021;34(10):2266-79. <https://doi.org/10.5829/ije.2021.34.10a.08>
30. Lee KL, Seed HB. Dynamic strength of anisotropically consolidated sand. *Journal of the Soil Mechanics and Foundations Division*. 1967;93(5):169-90. <https://doi.org/10.1061/JSFEAQ.0001019>
31. Seed HB. Earthquake-resistant design of earth dams. 1981.
32. Hosono Y, Yoshimine M, editors. Liquefaction of sand in simple shear condition. Proceedings of the international conference on cyclic behaviour of soils and liquefaction phenomena, Bochum, Germany; 2004. <https://doi.org/10.1201/9781439833452.ch16>
33. Hezarkhani A. Calculation of Mass Transfer and Element Mobility During the Hydrothermal Alteration in the Sungun PORPHYRY Copper Deposit Iran. *International Journal of Engineering*. 2002;15(4):391-408. https://www.ije.ir/article_71405_886c695fec0df2515fb2215538e9fa66.pdf
34. Ahmadi A, Bazaz JB. A new analytical model to predict the effect of suction removal on vacuum preloading of fine copper tailings. *Engineering Geology*. 2023;322:107176. <https://doi.org/10.1016/j.enggeo.2023.107176>
35. Ladd R. Preparing test specimens using undercompaction. *Geotechnical testing journal*. 1978;1(1):16-23. <https://doi.org/10.1520/GTJ10364J>
36. Karim ME, Alam M. Effect of nonplastic silt content on undrained shear strength of sand-silt mixtures. *International Journal of Geo-Engineering*. 2017;8(1):1-26. <https://doi.org/10.1186/s40703-017-0051-1>
37. Ishihara K, Tatsuoka F, Yasuda S. Undrained deformation and liquefaction of sand under cyclic stresses. *Soils and foundations*. 1975;15(1):29-44. <https://doi.org/10.3208/sandf1972.15.29>
38. Zhao J, Guo N. Unique critical state characteristics in granular media considering fabric anisotropy. *Géotechnique*. 2013;63(8):695-704. <https://doi.org/10.1680/geot.12.P.040>
39. Vaid YP, Chern J-C. Effect of static shear on resistance to liquefaction. *Soils and foundations*. 1983;23(1):47-60. <https://doi.org/10.3208/sandf1972.23.47>
40. Rasouli M, Moradi M, Ghalandarzadeh A. Effects of initial static shear stress orientation on cyclic behavior of calcareous sand. *Marine Georesources & Geotechnology*. 2021;39(5):554-68. <https://doi.org/10.1080/1064119X.2020.1726535>
41. Nadjafi M, Gholami P. Reliability Analysis of Notched Plates under Anisotropic Damage Based on Uniaxial Loading Using Continuum Damage Mechanics Approach. *International Journal of Engineering*. 2021;34(1):253-62. <https://doi.org/10.5829/ije.2021.34.01a.28>
42. Labibi H, Gerami M, Hosseini M. Sensitivity Analysis of Behavior of Simple Trapezoidal Steel Plates to Introduce a New Yielding Damper. *International Journal of Engineering*. 2021;34(10):2302-12. <https://doi.org/10.5829/ije.2021.34.10a.11>

- https://www.ije.ir/article_135667_63950229f30671722991ba6c2fc875a5.pdf
43. Ravikumar S, Kothandaraman S. Experimental Study on Performance of Ductile and Non-ductile Reinforced Concrete Exterior Beam-column Joint. *International Journal of Engineering*. 2022;35(7):1237-45. 10.5829/ije.2022.35.07a.03 https://www.ije.ir/article_147153_bc7874f6272869eca36d21efa0ff30c3.pdf
44. Danesh N, Mahmoodabadi MJ, Fathi AR. Investigation of the Damping Performance of a Shape Memory Alloy Beam. *International Journal of Engineering*. 2023;36(7):1369-82. 10.5829/ije.2023.36.07a.17 https://www.ije.ir/article_168122_470fa321ebd4ef0928a196fe888c0238.pdf
45. Javdanian H. Evaluation of soil liquefaction potential using energy approach: experimental and statistical investigation. *Bulletin of Engineering Geology and the Environment*. 2019;78(3):1697-708. <https://doi.org/10.1007/s10064-017-1201-6>

COPYRIGHTS

©2024 The author(s). This is an open access article distributed under the terms of the Creative Commons Attribution (CC BY 4.0), which permits unrestricted use, distribution, and reproduction in any medium, as long as the original authors and source are cited. No permission is required from the authors or the publishers.

**Persian Abstract****چکیده**

فعالیت های معدنی، از جمله اکتشاف، حفاری، و ساخت و ساز، اخیراً رشد چشمگیری داشته است. از این رو؛ استفاده از ضایعات معدنی با کمترین آسیب زیست محیطی یک نگرانی قابل توجه بوده است. سدهای باطله یکی از راه حل های رایجی است که زباله های حفاری را به منظور حفاظت از محیط زیست و حفظ منابع آب به صورت ایمن ذخیره می کند. این مقاله به عنوان مطالعه موردی به بررسی اثر بارهای یکنواخت و لرزه ای بر سیلت خالص مورد استفاده در یک سد باطله در شمال غرب ایران می پردازد. مقادیر مختلف تنش برشی استاتیک اولیه با استفاده از یک سیستم سه محوری سیکلی خودکار انجام می شود. آزمایش های فشاری زهکشی نشده مونوتونیک با تراکم نسبتاً ثابت و با در نظر گرفتن سه مقدار ۵۰، ۱۰۰ و ۱۵۰ کیلو پاسکال برای تنش مؤثر میانگین انجام شد. بسته به تراکم اولیه نمونه ها، با اعمال فشار محصور کننده موثر ۱۰۰ کیلو پاسکال، دانسیته های اولیه را بین ۲۵ تا ۳۰ درصد نسبت به شرایط اولیه افزایش داد. همچنین اثر نسبت تنش برشی استاتیکی اولیه با سه مقدار صفر، ۰/۲ و ۰/۴ نیز مورد ارزیابی قرار گرفت. هیچ نقطه ای اوجی برای نمونه های تحت شرایط $\alpha = 0$ مشاهده نشد، در حالی که، نمونه هایی با شرایط $\alpha = 0.4$ قبل از رسیدن به نقطه تبدیل فاز با یک نقطه اوج مواجه شدند. نتایج آزمایش های سیکلی به منظور ارزیابی انرژی ظرفیت و فشار منفذ باقی مانده بر اساس رویکرد انرژی کرنش استفاده شدند. آزمایش های سیکلی بر روی نمونه ها با در نظر گرفتن دامنه برشی ۰/۷۵ درصد و فرکانس ۰/۳ هرتز انجام گردید. نشان داده شده است که بیشترین اتلاف انرژی در اولین سیکل با بالاترین سختی رخ می دهد. برای $\alpha = 0$ ، چگالی انرژی از $474(J/m^3)$ به $1147/4(J/m^3)$ افزایش یافت، با این حال، افزایش شدیدتر در چگالی انرژی در شرایط $\alpha = 0.4$ از $682(J/m^3)$ به $5839(J/m^3)$ اندازه گیری گردید. همچنین مشخص شده است که اعمال تنش برشی اولیه تأثیر قابل توجهی بر مقاومت مونوتونیک و نیز مقاومت روانگرایی سیلت ها دارد. افزایش α از صفر به ۰/۴ باعث افزایش خطی مقاومت برشی نمونه ها در محدوده ۲۰ کیلو پاسکال تا ۷۰ کیلو پاسکال شد. سپس نتایج این مقاله از طریق برخی مطالعات قبلی به طور دقیق تأیید شدند.